Progress In Electromagnetics Research M, Vol. 79, 147–157, 2019

A Compact Endfire Radiation Antenna Based on Spoof Surface Plasmon Polaritons in Wide Bandwidth

Kaijie Zhuang[1], Jun-Ping Geng[1, *], Ziheng Ding[1], Xiaonan Zhao[2], Wenfeng Ma[3], Han Zhou[1], Chao Xie[1], Xianling Liang[1], and Rong-Hong Jin[1]

Abstract—A compact slot-coupled endfire radiation antenna based on a tapering spoof surface plasmon polaritons (SSPPs) structure with high efficiency is proposed in this paper. A narrow slot balun is designed to feed the SSPPs structure rather than to work as the primary radiator. Simulated results show that the odd SPP mode is successfully excited on the tapering SSPPs structure, which contributes to the endfire radiation. Due to the high confinement of SSPPs, the proposed antenna shows low RCS within the frequency band of 1.5 GHz–4 GHz and 5.6 GHz–8 GHz. A prototype is fabricated and tested. Simulated and measured results show good agreement that the proposed antenna can provide stable endfire radiation patterns within the frequency band of 2 GHz–3.4 GHz. The maximum gain reaches 8 dBi, and the average efficiency over this bandwidth is 80%. The high-efficiency endfire SSPPs antenna with balanced broad band and high gain has a promising application in communication systems and integrated circuits.

1. INTRODUCTION

Surface plasmon polaritons (SPPs) are special electromagnetic (EM) waves bound on the interface of two materials where the real parts of permittivity are opposite in sign [1–8]. The use of SPPs in technology has originated the novel research field of plasmonics, whose applications are found in several fields ranging from optoelectronics [9–13], nanomedicine [14–18], and membrane technology [19–21]. Many antennas have been reported based on plasmonics, but they are designed for optical regions [22–25]. Based on the valuable work in [26] and [27], spoof SPPs (SSPPs) have been realized in the microwave band by using structured surfaces. Afterward, SSPPs have inspired intensive interest in microwave community. Extensive applications based on SSPPs waveguide have been reported, including transmission line [28–30], filters [31–33], and wave splitters [34–36].

Due to the strong field-confinement characteristic and phase mismatch with free space, the electromagnetic wave supported on SSPPs transmission line does not radiate, which limits the application of the SSPPs in antenna design to a certain extent. With tapering structures [40, 41], or resonating elements [42–44], or periodic modulations [37–39], SSPPs modes can be converted into spatial radiated modes.

Many valuable works on SSPPs antennas have been reported [37–47]. In [38], a leaky wave antenna based on SSPPs is proposed, in which periodically loaded patches are introduced to provide an additional momentum for phase matching with the radiated waves in the space. In [39], an asymmetrical plasmonic waveguide is reported to improve the radiation efficiency of the periodically modulated SSPPs leaky wave antenna. A new method is proposed to efficiently radiate electromagnetic (EM) wave form SSPPs

Received 14 December 2018, Accepted 30 January 2019, Scheduled 14 March 2019
* Corresponding author: Jun-Ping Geng (gengjunp@sjtu.edu.cn).
[1] Department of Electronics Engineering, Shanghai Jiao Tong University Shanghai 200240, China. [2] China Ship Development and Design Center, Wuhan 430060, China. [3] PLA Army Engineering University, Jiangsu, Nanjing 21007, China.

structure, as presented in [43]. A flaring metal structure is introduced to realize wide band impedance matching.

All the SSPPs antennas reported so far are dedicated to realizing efficient conversion of SSPPs modes to spatial radiated modes, and most of them steer the beam around the broadside. In [41], an endfire SSPPs antenna is reported. This antenna is fed by a monopole, and a tapering structure [48, 49] is used to couple the electromagnetic wave from the monopole. The odd surface wave mode is excited along the SSPPs structure and is radiated through the tapering structure at the end. This antenna shows good radiation patterns in the endfire direction. Owing to the resonant nature of the monopole, it exhibits a narrow frequency band. Another endfire radiation antenna based on SSPPs is presented in [42]. Similar to the antenna reported in [41], this antenna shows a narrow impedance band. To improve the impedance band of endfire SSPPs antenna, a traveling-wave antenna for endfire radiation is proposed [40]. This antenna provides an endfire radiation beam within 7.5–8.5 GHz. However, due to the traveling-wave characteristic, there are many side lobes. It is noted that the corrugated edges used in Vivaldi antennas are designed to suppress the surface wave [50, 51], and the SSPPs are not exactly excited.

In this paper, we propose an efficient compact SSPPs endfire antenna over a wide operating frequency band. This antenna is mainly composed of a transition area, tapering SSPPs structure, and microstrip feed line. The narrow extending slot in the tapering SSPPs structure works as a running waveguide, and the triangular slot at the end of the antenna is introduced to improve the impedance matching and radiation performance. The odd SSPPs mode is excited through the narrow slot, and the tapering structure is designed to convert the SSPPs mode to spatial radiated mode. Unlike Vivaldi antennas where slot is the primary radiator, the narrow slot in this design cannot provide an endfire radiation beam over a wide frequency band, and the corrugated SSPPs structure is introduced as a main radiator to couple the energy from the slot. Due to the high confinement of SSPPs, EM wave is transmitted and radiated to the endfire direction. The proposed antenna shows good radiation patterns in the endfire direction within a wide operating band of 2–3.4 GHz. Furthermore, because of the advantages of SSPPs, the proposed antenna exhibits the characteristic of low profile and high field-confinement, which could be fabricated close to each other without significant mutual coupling [52]. In addition, SSPPs structure can also reduce antenna RCS within the frequency bands of 1.5 GHz–4 GHz and 5.6 GHz–8 GHz. The proposed antenna shows high directivity in endfire direction with an average radiation efficiency about 80% in the available band. The work in this paper provides an efficient method to feed SSPPs antenna and is of great value in communication systems and integrated circuits.

The structure and key parameters of the proposed antenna are explained in Section 2. Antenna prototype and experimental results are discussed in Section 3. Finally, the conclusion is given in Section 4.

2. ANTENNA DESIGN AND ANALYSIS

2.1. Antenna Structure and Principle

The configuration of the proposed SSPPs endfire antenna is shown in Figure 1. The entire metal structure is fabricated on a 0.762-mm-thick Arlon AD250 substrate (with $\varepsilon_r = 2.5$ and $\tan\sigma = 0.0018$). The tapering microstrip line at the back of the antenna is designed to feed the narrow extending slot as shown in Figure 1(b). The microstrip line is designed to match the impedance of 50 Ω.

Compared with conventional microstrip line, the arc-shaped tapering microstrip line provides a better impedance matching. A fan-shaped patch is loaded at the end of the microstrip line to improve antenna efficiency. r_2 is the radius of this fan-shaped patch. The narrow extending slot in the part of SSPPs structure works as a waveguide for the running wave, and the triangular slot at the end of the antenna is introduced to reduce the reflection. L_3 and W_2 are the height and bottom side of the triangle.

By introducing the SSPPs structure, the EM wave supported on the narrow slot is coupled to the tapering SSPPs structure. The electric fields on the tapering SSPPs structure is anti-symmetric (odd mode [30]), which contributes to the endfire radiation together with the narrow slot.

The exponential profile curve is employed in the design of SSPPs transmission line to improve the

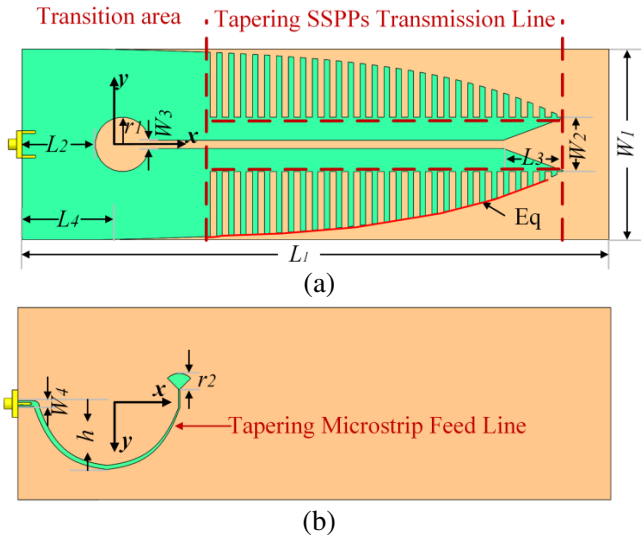

Figure 1. Proposed endfire radiation antenna. (a) Front view, (b) back view of the proposed antenna.

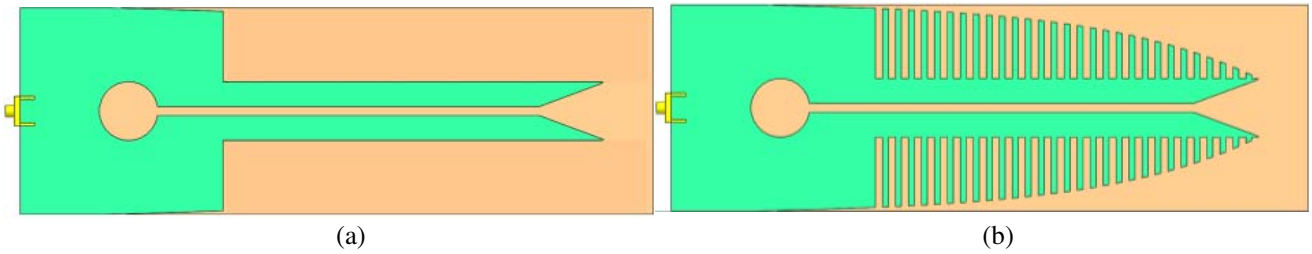

Figure 2. (a) Narrow slot antenna, (b) the proposed SSPPs antenna.

antenna performance. The ridge curve equation is defined as

$$y = e^{ln(0.5\times W_1+1)\times[(x-L_4)/(L_1-L_4)]} - 1 - 0.5 \times W_1 \quad (L_4 \le x \le L_1) \tag{1}$$

2.2. Simulation Verification and Parameter Analysis

A series of simulations have been performed using CST Microwave Studio. Figure 2 shows the structure of a narrow slot antenna and the proposed SSPPs antenna. $|S_{11}|$ performances of these two antennas are compared in Figure 3. $|S_{11}|$ means the input return loss at the antenna port. The lower the $|S_{11}|$ value is, the more the energy is fed into the antenna. $|S_{11}|$ performance affects the antenna efficiency and is recommended below -10 dB. It is observed that $|S_{11}|$ performance is significantly improved with SSPPs structure.

On the other hand, the narrow slot works as a waveguide for the running wave, and it can provide an endfire beam within a very narrow band at 2.5 GHz from the simulation results. The power flow distributions at 2.5 GHz of these two antennas are compared in Figure 4. It can be seen from Figure 4 that part of the EM energy in the narrow slot antennas is radiated to the endfire direction, and the rest of the EM energy is transmitted to the opposite direction from the end of the slot. However, the EM energy in the proposed SSPPs antenna is gradually coupled from the slot to the SSPPs structure and radiated to the endfire direction.

The electric field distribution is shown in Figure 5(a). It is clear that the dominant surface wave mode transmitted on the structure is odd mode [30] rather than the even mode on conventional plasmonic metamaterials [39, 44]. The radiation pattern at 2.5 GHz is presented in Figure 5(b) which shows good endfire radiation patterns. The simulated antenna gain reaches 7.28 dBi and is with low side lobes.

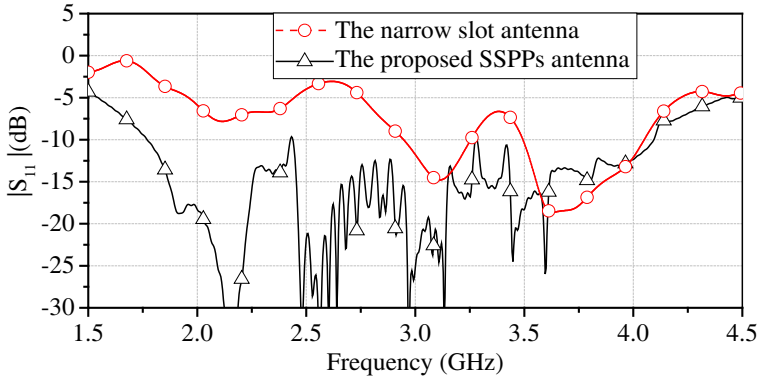

Figure 3. Comparison of the $|S_{11}|$ performance between the narrow slot antenna and the proposed SSPPs antenna.

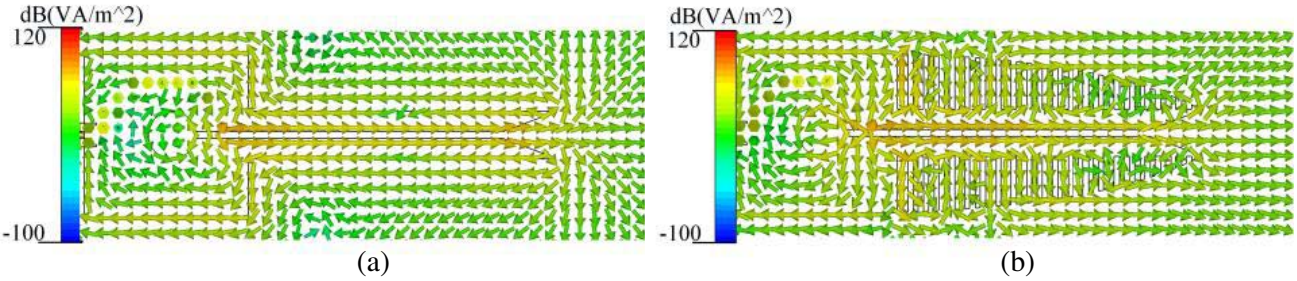

Figure 4. The power flow of (a) narrow slot antenna, (b) the proposed SSPPs antenna at 2.5 GHz, respectively.

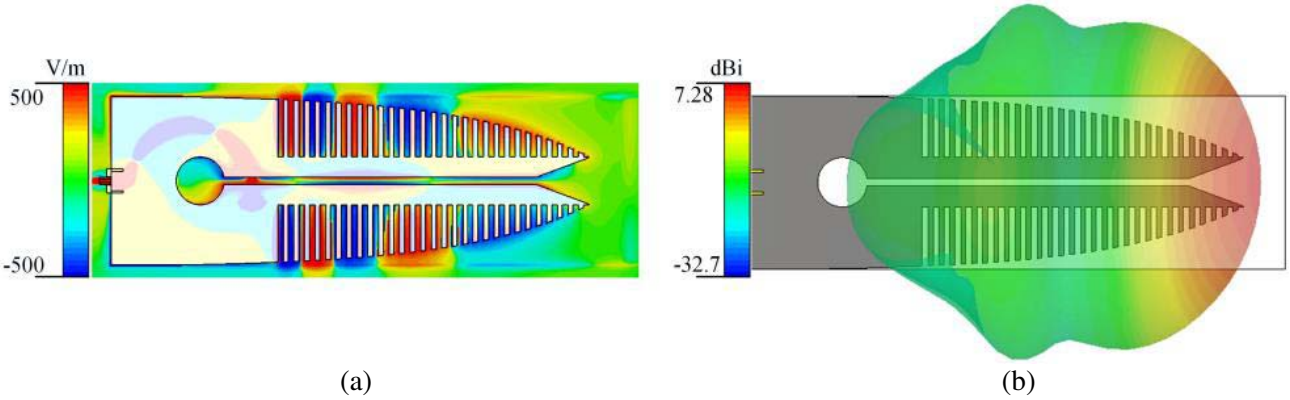

Figure 5. (a) Electric field (Ez component) distribution near the structure at 2.5 GHz, (b) radiation pattern at 2.5 GHz.

The RCSs versus frequency are compared in Figure 6. The gray area is the impedance band of the proposed SSPPs antenna and a same size Vivaldi antenna. It is observed that both the proposed SSPPs antenna and Vivaldi antenna can reduce RCS within the operating band of 1.5 GHz–4 GHz. On the other hand, RCS of the Vivaldi antenna is above −10 dB and is close to that of a metallic plate within the frequency band of 5.6 GHz–8 GHz, but within this band, the RCS could be significantly reduced due to the high confinement of the SSPPs.

In Figure 7, $|S_{11}|$ performances of the proposed antenna with and without the triangle slot at the end are compared. It can be observed that $|S_{11}|$ performance is significantly improved by introducing

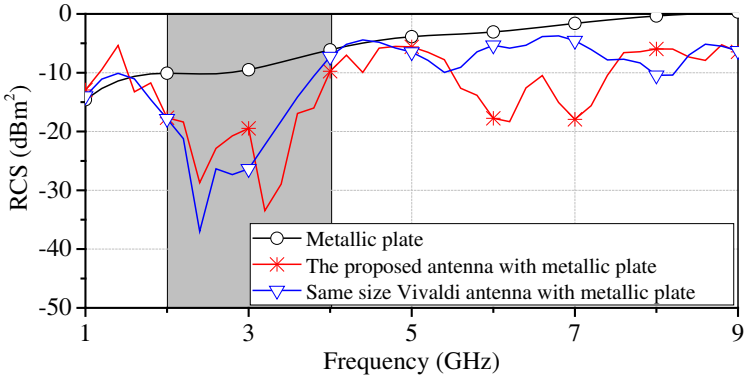

Figure 6. The simulated RCS versus frequency (y-polarization), (a) a metallic square plate with a side of 100 mm, (b) the proposed SSPPs antenna with a metallic plate, (c) a same size Vivaldi antenna with a metallic plate.

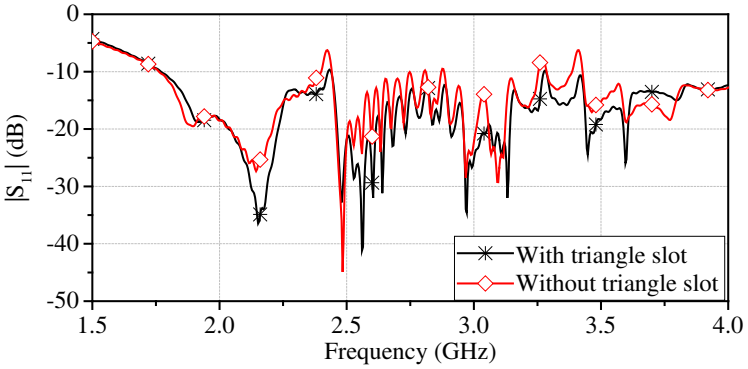

Figure 7. Comparison of $|S_{11}|$ performance with and without the triangle slot at the end.

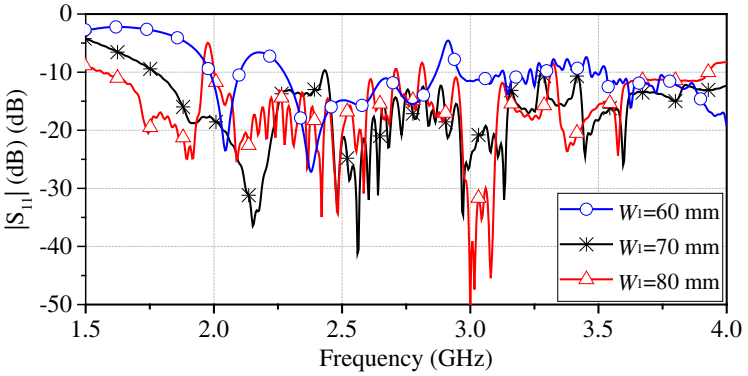

Figure 8. Effect of W_1 on the $|S_{11}|$ performance.

the triangle slot. The tapering structure is important to the antenna impedance matching. In Figure 8, $|S_{11}|$ performances are compared versus the variable of W_1. It is observed that if W_1 increases, the operating band will move to the lower band. If W_1 decreases from 70 mm to 60 mm or increases from 70 mm to 80 mm, $|S_{11}|$ performance will deteriorate. Figure 9 compares $|S_{11}|$ values versus L_1, and the frequency band is stable as L_1 increases from 210 mm to 220 mm, but if L_1 decreases to 200 mm, the impedance matching will deteriorate. Considering the antenna size, $L_1 = 210$ mm is a better choice.

The proposed endfire antenna is designed through a series of simulations. The optimized values of parameters are listed in Table 1.

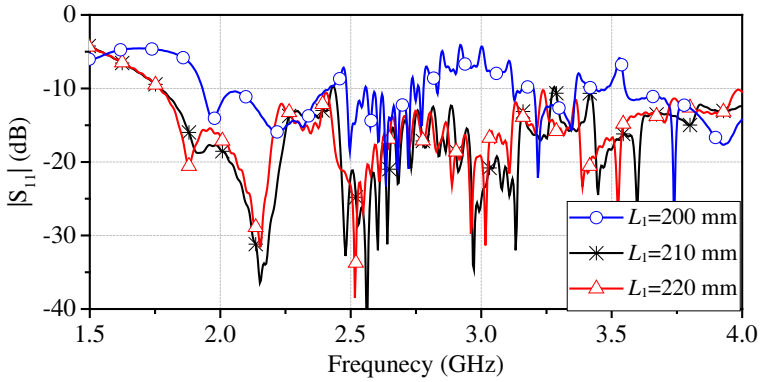

Figure 9. Effect of L_1 on the $|S_{11}|$ performance.

Table 1. Optimized geometric parameters of the pattern reconfigurable antenna.

Parameters	h	L_1	L_2	L_3
Values/mm	25	216	27.1	20.6
Parameters	L_4	r_1	r_2	W_1
Values/mm	29	10	6	70
Parameters	W_2	W_3	W_4	
Values/mm	3	2.1	19.6	

3. EXPERIMENTAL RESULT AND DISCUSSION

A prototype was fabricated and measured. The simulated and measured $|S_{11}|$ curves of the proposed endfire antenna are compared in Figure 10. It is observed that the simulated 10-dB impedance bandwidth is about 2.3 GHz over 1.8–4.1 GHz (about 78%). Also, the measured 10-dB impedance bandwidth of the proposed antenna covers 1.8–4.3 GHz (about 82%). The measured results agree well with the simulated ones.

The simulated and measured antenna efficiencies and realized gains versus frequency are given in Figure 11. It is observed that the simulated average efficiency is above 97%, and the measured radiation efficiency is around 80%. The measured and simulated gains match well with each other within the operating band of 2–3.4 GHz except 3.1 GHz. Because the measured efficiency declines at 3.1 GHz, the

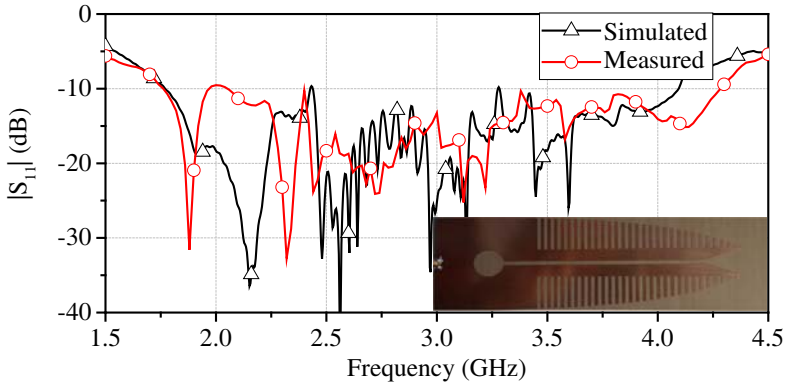

Figure 10. Comparison of the simulated and measured $|S_{11}|$ values of the proposed endfire antenna.

measured gain deteriorates accordingly. It is also observed that the simulated antenna gain at 2.3 GHz and 2.4 GHz is smaller than that at other frequencies without obvious efficiency decline. It is because the EM wave transmitted on the narrow slot is huge at these frequencies, and the surface wave out of the narrow slot suppresses the SSPPs through the triangle slot. Thus the beam is widened, and the antenna gain declines. At other frequencies, the SSPPs work as the dominant radiator, and the extending antenna aperture makes the radiation beam become narrow, resulting in high realized gain.

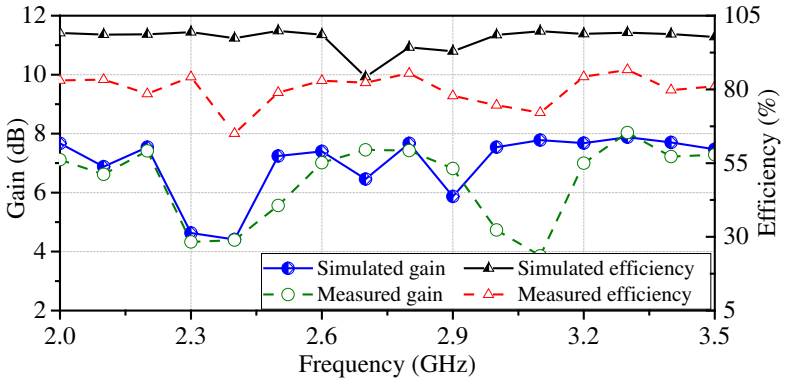

Figure 11. Comparison of the simulated and measured gain and efficiency of the proposed endfire antenna.

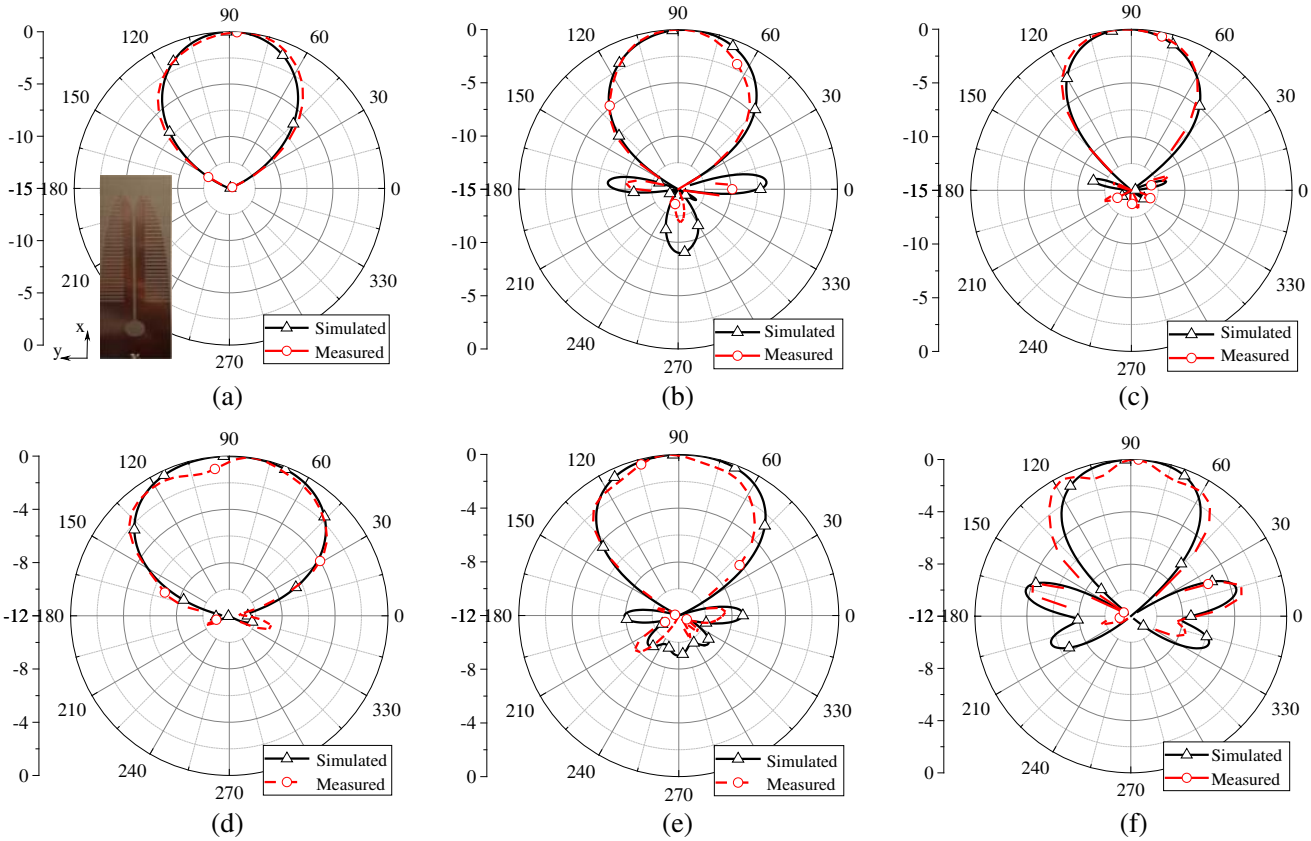

Figure 12. Simulated and measured radiation patterns of the proposed endfire antenna. (a), (b) and (c) show the radiation pattern in the *xoy* plane at 2 GHz, 2.7 GHz, and 3.4 GHz, respectively; (d), (e) and (f) show the radiation pattern in the *xoz* plane at 2 GHz, 2.7 GHz, and 3.4 GHz, respectively.

The proposed antenna can provide endfire radiation beams within the frequency range from 2 GHz to 3.4 GHz. Radiation patterns in the *xoy* plane are given in Figure 12, in which Figures 12(a), (b), and (c) show good radiation patterns in the *xoy* plane at 2 GHz, 2.7 GHz, and 3.4 GHz, respectively, and Figures 12(d), (e), and (f) show good radiation patterns in the *xoz* plane at 2 GHz, 2.7 GHz, and 3.4 GHz, respectively. It is observed that the measured results match well with the simulated ones.

Table 2. Performance comparison of endfire antennas.

Ref.	Bands (GHz)	Size	Peak gain (dBi)	Radiation efficiency
[40]	7.5–8.5	$2.9\lambda_c \times 0.8\lambda_c$	9.2	96%
[41]	9–10.5	$3.6\lambda_c \times 0.5\lambda_c$	~ 9.7	high
[42]	6	$2.3\lambda_c \times 0.6\lambda_c$	7	92.3%
[51]	0.5–6	$2.8\lambda_c \times 1.6\lambda_c$	~ 8	-
This letter	2–3.4	$1.9\lambda_c \times 0.6\lambda_c$	8	80%

$*\lambda_c$ is the wavelength at the center frequency.

The performances of our prototype and other different types of previously reported SSPPs endfire antennas [40–42] are compared in Table 2. A UWB Vivaldi antenna reported in [51] is also compared in Table 2. The proposed endfire SSPPs antenna size is $1.9\lambda_c \times 0.6\lambda_c$, peak gain 8 dBi, and average efficiency 80% over 2–3.4 GHz. It is observed that compared with the other SSPPs endfire antennas reported in [40–42], the proposed design achieves the most compact size and the widest frequency band. The realized gain is relatively high with respect to the antenna size. Compared to the miniaturized Vivaldi antenna [51], the realized gain of the proposed antenna is relatively high and less fluctuating.

4. CONCLUSION

An efficient compact SSPPs endfire antenna over wide operating frequency band is studied. The microstrip is used to feed the narrow extending slot and to excite the odd SSPPs mode, which supports the endfire radiation pattern. Due to the high confinement of SSPPs, the proposed antenna shows low RCS within the frequency bands of 1.5 GHz–4 GHz and 5.6 GHz–8 GHz. The manufactured prototype of the proposed antenna realizes endfire radiation beam within a wide frequency band of 2–3.4 GHz. The measured maximum gain reaches 8 dBi, and the average efficiency is 80% over the operating band. Ease of fabrication, low profile, and high efficiency render this antenna highly suitable for endfire applications.

ACKNOWLEDGMENT

This work was supported by the National Natural Science Foundation of China under Grants 61571289, 61571298 and 61701303, and Shanghai Pujiang Program (17PJ1404100).

REFERENCES

1. Barnes, W. L., A. Dereux, and T. W. Ebbesen, "Surface plasmon sub-wavelength optics," *Nature*, Vol. 424, 824–830, Aug. 2003.
2. Sarkar, T. K., et al., "Surface plasmons/polaritons, surface waves, and zenneck waves: Clarification of the terms and a description of the concepts and their evolution," *IEEE Antennas & Propagation Magazine*, Vol. 59, 77–93, Jun. 2017.
3. Grigorenko, A. N., M. Polini, and K. S. Novoselov, "Graphene plasmonics," *Nat. Photonics*, Vol. 6, 749–758, Nov. 2012.
4. Politano, A., G. Chiarello, and C. Spinella, "Plasmon spectroscopy of graphene and other two-dimensional materials with transmission electron microscopy," *Mater. Sci. Semicond. Process.*, Vol. 65, 88–99, Jul. 2017.

5. Politano, A. and G. Chiarello, "Plasmon modes in graphene: status and prospect," *Nanoscale*, Vol. 6, 10927–10940, Jul. 2014.
6. Tassin, P., T. Koschny, M. Kafesaki, and G. M. Soukoulis, "A comparison of graphene, superconductors and metals as conductors for metamaterials and plasmonics," *Nat. Photonics*, Vol. 6, 259–264, Mar. 2012.
7. Bao, Q. and K. P. Loh, "Graphene photonics, plasmonics, and broadband optoelectronic devices," *ACS Nano*, Vol. 6, No. 5, 3677–3694, Apr. 2012.
8. Koppens, F. H. L., D. E. Chang, and F. J. G. D. Abajo, "Graphene plasmonics: A platform for strong light-matter interactions," *Nano Lett.*, Vol. 11, No. 8, 3370–3377, Jul. 2011.
9. Politano, A., L. Viti, and M. S. Vitiello, "Optoelectronic devices, plasmonics, and photonics with topological insulators," *APL Materials*, Vol. 5, Feb. 2017.
10. Viti, L., J. Hu, D. Coquillat, A. Politano, W. Knap, and M. S. Vitiello, "Efficient Terahertz detection in black-phosphorus nano-transistors with selective and controllable plasma-wave, bolometric and thermoelectric response," *Sci. Rep.*, Vol. 6, Feb. 2016.
11. Viti, L., D. Coquillat, A. Politano, K. A. Kokh, Z. S. Aliev, Z. S. Aliev, M. B. Babanly, O. E. Tereshchenko, W. Knap, E. V. Chulkov, and M. S. Vitiello, "Plasma-wave terahertz detection mediated by topological insulators surface states," *Nano Lett.*, Vol. 16, No. 1, 80–87, Dec. 2015.
12. Berry, C. W., N. Wang, M. R. Hashemi, M. Unlu, and M. Jarrahi, "Significant performance enhancement in photoconductive terahertz optoelectronics by incorporating plasmonic contact electrodes," *Nat. Commun.*, Vol. 4, Mar. 2013.
13. Tang, W., A. Politano, C. Guo, W. Guo, C. Liu, L. Wang, X. Chen, and W. Lu, "Ultrasensitive room]temperature terahertz direct detection based on a bismuth selenide topological insulator," *Adv. Funct.*, Vol. 28, No. 31, Aug. 2018.
14. Agarwal, A., M. S. Vitiello, L. Viti, A. Cupolilloc, and A. Politano, "Plasmonics with two-dimensional semiconductors: from basic research to technological applications," *Nanoscale*, Vol. 10, 8938–8946, May, 2018.
15. Ali, M. R. K., H. R. Ali, C. R. Rankin, and M. A. El-Sayed, "Targeting heat shock protein 70 using gold nanorods enhances cancer cell apoptosis in low dose plasmonic photothermal therapy," *Biomaterials*, Vol. 102, 1–8, Sep. 2016.
16. Law, W. C., K. T. Yong, A. Bae, and P. N. Prasad, "Sensitivity improved surface plasmon resonance biosensor for cancer biomarker detection based on plasmonic enhancement," *ACS Nano*, Vol. 5, No. 6, 4858–4864, Apr. 2011.
17. Zhang, J. Z., "Biomedical applications of shape-controlled plasmonic nanostructures: A case study of hollow gold nanospheres for photothermal ablation therapy of cancer," *J. Phys. Chem. Lett.*, Vol. 1, No. 4, 686–695, Jan. 2010.
18. Wang, H. N. and T. Vo-Dinh, "Multiplex detection of breast cancer biomarkers using plasmonic molecular sentinel nanoprobes," *Nanotechnology*, Vol. 20, No. 6, Jan. 2009.
19. Politano, A., G. D. Profio, E. Fontananova, V. Sanna, A. Cupolillo, and E. Curcio, "Overcoming temperature polarization in membrane distillation by thermoplasmonic effects activated by Ag nanofillers in polymeric membranes," *Desalination*, Vol. 451, 192–199, Feb. 2019.
20. Politano, A., P. Argurio, G. D. Profio, V. Sanna, A. Cupolillo, S. Chakraborty, H. A. Arafat, and E. Curcio, "Photothermal membrane distillation for seawater desalination," *Adv. Mater.*, Vol. 29, No. 2, Jan. 2017.
21. Politano, A., A. Cupolillo, G. Di Profio, H. A. Arafat, G. Chiarello and E. Curcio, "When plasmonics meets membrane technology," *J. Phys.: Condens. Matter*, Vol. 28, No. 36, Jul. 2016.
22. Park, K. D. and M. B. Raschke, "Polarization control with plasmonic antenna tips: A universal approach to optical nano-crystallography and vector-field imaging," *Nano Lett.*, Vol. 18, No. 5, 2912–2917, Mar. 2018.
23. Xu, W., T. K. Lee, B. S. Moon, H. Song, X. Chen, B. Chun, Y. J. Kim, S. K. Kwak, P. Chen, and D. H. Kim, "Broadband plasmonic antenna enhanced upconversion and its application in flexible fingerprint identification," *Adv. Opt. Mater.*, Vol. 6, No. 6, Mar. 2018.

24. Vercruysse, D., P. Neutens, L. Lagae, N. Verellen, and P. V. Dorpe, "Single asymmetric plasmonic antenna as a directional coupler to a dielectric waveguide," *ACS Photonics*, Vol. 4, No. 6, 1298–1402, Apr. 2017.
25. Viti, L., J. hu, D. Coquillat, W. Knap, A. Tredicucci, A. Polotano, and M. S. Vitiello, "Black phosphorus terahertz photodetectors," *Adv. Mater.*, Vol. 27, 5567–5572, May 2018.
26. Pendry, J., L. Martin-Moreno, and F. Garcia-Vidal, "Mimicking surface plasmons with structured surfaces," *Science*, Vol. 305, 847–848, 2004.
27. Maier, S. A., S. R. Andrews, L. Martin-Moreno, and F. Garcia-Vidal, "Terahertz surface plasmon-polariton propagation and focusing on peri-odically corrugated metal wires," *Phys. Rev. Lett.*, Vol. 97, Oct. 2006.
28. Kianinejad, A., Z. N. Chen, and C. W. Qiu, "Low-loss spoof surface plasmon slow-wave transmission lines with compact transition and high isolation," *IEEE Transactions on Microwave Theory Techniques*, Vol. 64, No. 10, 3078–3086, 2016.
29. Liu, L., et al., "Dual-band trapping of spoof surface plasmon polaritons and negative group velocity realization through microstrip line with gradient holes," *Applied Physics Letters*, Vol. 107, No. 20, 2015.
30. Gao, X., L. Zhou, and T. J. Cui, "Odd-mode surface plasmon polaritons supported by complementary plasmonic metamaterial," *Scientific Reports*, 2015.
31. Yin, J. Y., J. Ren, H. C. Zhang, B. C. Pan, and T. J. Cui, "Broadband frequency-selective spoof surface plasmon polaritons on ultrathin metallic structure," *Sci. Rep.*, Vol. 5, 2015.
32. Pan, B. C., Z. Liao, J. Zhao, and T. J. Cui, "Controlling rejections of spoof surface plasmon polaritons using metamaterial particles," *Opt. Express*, Vol. 22, 13940–13950, Jun. 2014.
33. Wu, J. J., D. J. Hou, T. Yang, I. Hsieh, Y. Kao, and H. Lin, "Bandpass filter based on low frequency spoof surface plasmon polaritons," *Electron. Lett.*, Vol. 48, 269–270, Mar. 2012.
34. Shibayama, J., J. Yamauchi, and H. Nakano, "Metal disc-type splitter with radially placed gratings for terahertz surface waves," *Electron. Lett.*, Vol. 51, 352–353, Feb. 2015.
35. Shen, X., G. Moreno, A. Chahadih, T. Akalin, and T. J. Cui, "Spoof surface plasmonic devices and circuits in THz frequency," *IRMMW-THz*, 1, 2014
36. Zhou, Y. J., X. X. Yang, and T. J. Cui, "A multidirectional frequency splitter with band-stop plasmonic filters," *Journal of Applied Physics*, Vol. 115, No. 12, 2014.
37. Liao, D., Y. Zhang, and H. G. Wang, "Wide-angle frequency-controlled beam scanning antenna fed by standing wave based on the cut-off characteristics of spoof surface plasmon polaritons," *IEEE Antennas & Wireless Propagation Letters*, Vol. 17, No. 7, Jul. 2018.
38. Zhang, Q., Q. Zhang, and Y. Chen, "Spoof surface plasmon polariton leaky-wave antennas using periodically loaded patches above PEC and AMC ground planes," *IEEE Antennas Wireless Propag. Lett.*, Vol. 16, 3014–3017, 2017.
39. Gu, S. K., H. F. Ma, B. G. Cai, and T. J. Cui, "Continuous leaky-wave scanning using periodically modulated spoof plasmonic waveguide," *Scientific Reports*, Vol. 6, 29600, 2016.
40. Kandwal, A., Q. Zhang, X. Tang, L. W. Liu, and G. Zhang, "Low-profile spoof surface plasmon polaritons traveling-wave antenna for endfire radiation," *IEEE Antennas Wireless Propag. Lett.*, Vol. 17, No. 2, 184–187, 2017.
41. Han, Y. J., et al., "360° scanning multi-beam antenna based on spoof surface plasmon polaritons," *Acta Physica Sinica*, Vol. 65, No. 14, 2016.
42. Yin, J. Y., D. Bao, J. Ren, H. C. Zhang, B. C. Pan, Y. Fan, and T. J. Cui, "Endfire radiations of spoof surface plasmon polaritons," *IEEE Antennas and Wireless Propagation Letters*, Vol. 16, 597–600, 2017.
43. Yin, J. Y., et al., "Direct radiations of surface plasmon polariton waves by gradient groove depth and flaring metal structure," *IEEE Antennas & Wireless Propagation Letters*, Vol. 15, 865–868, 2016.
44. Dong, W., et al., "A high efficiency broadband omnidirectional UHF patch antenna applying surface plasmon polaritons for handheld terminals," *IEEE Antennas & Wireless Propagation Letters*,

Vol. 17, 283–286, 2018.

45. Dong, W., et al., "A novel patch antenna based on surface plasma polarization," *The 5th International Symposium on Electromagnetic Compatibility, EMC*, Beijing, Oct. 2017.
46. Dong, W., et al., "A surface plasmon polariton inspired patch antenna," *IEEE APS*, San Diago, 2017.
47. Zhuang, K., et al., "Spoof surface plasmon polaritons pattern reconfigurable antenna for wide-angle coverage," *IEEE APS*, 2018.
48. Zhang, J., L. Cai, W. Bai, Y. Xu, and G. Song, "Slow light at terahertz frequencies in surface plasmon polariton assisted grating waveguide," *Journal of Applied Physics*, Vol. 106, No. 10, Nov. 2009.
49. Xiang, H., Y. Meng, Q. Zhang, F. F. Qin, J. J. Xiao, D. Han, and W. Wen, "Spoof surface plasmon polaritons on ultrathin metal strips with tapered grooves," *Optics Communications*, Vol. 356, No. 1, 59–63, Dec. 2015.
50. Zhang, Y., E. Li, C. Wang, and G. Guo, "Radiation enhanced Vivaldi antenna with double-antipodal structure," *IEEE Antennas & Wireless Propagation Letters*, Vol. 16, No. 99, 561–564, 2017.
51. Liu, Y., W. Zhou, S. Yang, W. Li, P. Li, and S. Yang, "A novel miniaturized vivaldi antenna using tapered slot edge with resonant cavity structure for ultra-wide band applications," *IEEE Antennas and Wireless Propagation Letters*, 2016.
52. Kianinejad, A., Z. N. Chen, and C.-W. Qiu, "Design and modeling of spoof surface plasmon modes-based microwave slow-wave trans-mission line," *IEEE Trans. Microw. Theory Tech.*, Vol. 63, No. 6, 1817–1825, Jun. 2015.